Electronic origin of the spin-phonon coupling effect in transition-metal perovskites

Hongwei Wang, Lixin He, Hong Jiang, Cameron Steele, and Xifan Wu

Phys. Rev. B **96**, 075121 — Published 11 August 2017

DOI: 10.1103/PhysRevB.96.075121

Electronic origin of spin-phonon coupling effect in transition-metal perovskites

Hongwei Wang[1,2], Lixin He[1,*], Hong Jiang[3], Cameron Steele[2], and Xifan Wu[2,*]
[1] *Key Laboratory of Quantum Information, University of Science and Technology of China, Hefei, Anhui 230026, China*
[2] *Department of Physics, Temple University, 1925 N 12th Street, Philadelphia, Pennsylvania 19122, USA and*
[3] *Beijing National Laboratory for Molecular Sciences, College of Chemistry and Molecular Engineering, Peking University, 100871 Beijing, China*
(Dated: July 27, 2017)

By applying Wannier-based extended Kugel-Khomskii model, we carry out first-principles calculations and electronic structure analysis to understand the spin-phonon coupling effect in transition-metal perovskites. We demonstrate the successful application of our approach to $SrMnO_3$ and $BiFeO_3$. We show that both the electron orbitals under crystal field splitting and the electronic configuration should be taken into account in order to understand the large variances of spin-phonon coupling effects among various phonon modes as well as in different materials.

PACS numbers: 75.85.+t, 77.80.-e, 77.84.Lf

I. INTRODUCTION

Spin-phonon coupling (SPC) is an important physical effect of multiferroic materials[1], in which the cross couplings between structural distortions and magnetic orderings are closely associated with their key functionalities, such as magnetoelectric coupling. Due to its fundamental and technological importance, the SPC effect is currently under intense scientific investigations[2–5].

The mechanism in realizing SPC is not obviously accessible since the structural distortion, in particular ferroelectricity (FE) does not necessarily induce a change of the magnetic interaction of the material. SPC can be realized by the relativistic effect through the spin-orbital interaction. FE was induced by the spin spiral structure that breaks the inversion symmetry[6], or the crystal structure in improper multiferroics can be compatible with spin configurations generating the weak ferromagnetism (FM)[7,15,16]. Unfortunately, the resulting electric and magnetic moments are generally small. Recently, a new SPC mechanism has been discovered in transition metal ABO_3 perovskites [17–24]. It was found that the low-lying phonon modes, particularly the polar ones, are significantly softened when the spin coupling is changed from being antiferromagnetic (AFM) to FM.

By predicting phonon frequencies under different magnetic orderings, first-principles calculations have pioneered the search for SPC materials. As a result, a number of transition-metal perovskites with SPC effect have been identified[17–19]. Notwithstanding the progress in the field, several fundamental properties remain to be understood. First, for a single material, the SPC strength varies significantly in terms of the computed shifted phonon frequencies among different phonon modes[25–27]. Second, SPC is not observed as a general property for multiferroic materials. In particular, $BiFeO_3$ (BFO) as one of the most studied room temperature multiferroic materials has surprisingly weak SPC effect[28,29]. Based on the Goodenough-Kanamori-Anderson (GKA) rules, the metal-oxygen-metal angles are often used to explain the SPC effect[30,31]; however, such a phenomenological argument only roughly captures the effect which is neither accurate or conclusive. Precise assignments of electronic processes involved in the magnetic exchange interactions and their couplings to phonon modes are keys in addressing the above questions.

Here, we elucidate the electronic origins of SPC effect by using $SrMnO_3$ (SMO) and BFO as examples. In particular, we compute the superexchange (SE) interactions via the virtual electronic hopping processes with a recently developed extended Kugel-Khomskii (KK) model[32] based on maximally localized Wannier functions (MLWFs)[33,34], in which the electronic screening is considered by constrained random phase approximation(cRPA)[35]. The SPC effect can be understood as the tendency towards the suppressed SE interaction under the structural distortion along the phonon mode. The electronic structure plays a crucial role in these processes. On one hand, phonon modes that effectively change the hybridization between Mn-3d and O-2p are found to have strong SPC effect via the hopping integrals. On the other hand, the rather different details in the virtual hopping processes originating from the distinct electronic configurations in Mn^{4+} and Fe^{3+} ions explain the much weaker SPC effect in BFO than that of SMO. Our results bridge the gap between the GKA phenomenological rule and electronic structure of materials, and provide important guidance to the search for new SPC materials.

II. WANNIER-BASED KUGEL-KHOMSKII MODEL

As a prototypical example, the SPC effect in cubic SMO can be clearly seen by the softening of low lying phonon frequencies when the spin coupling is changed from AFM to FM as shown in Table I. The Slater, Axe, and Last modes[36–38] are all polar modes originating from the Gamma point instabilities; the antiferrodistortive (AFD) mode refers to the oxygen octahedral rotation mode originating from the Brillouin zone boundary instability[39,40]. The phonon frequency soft-

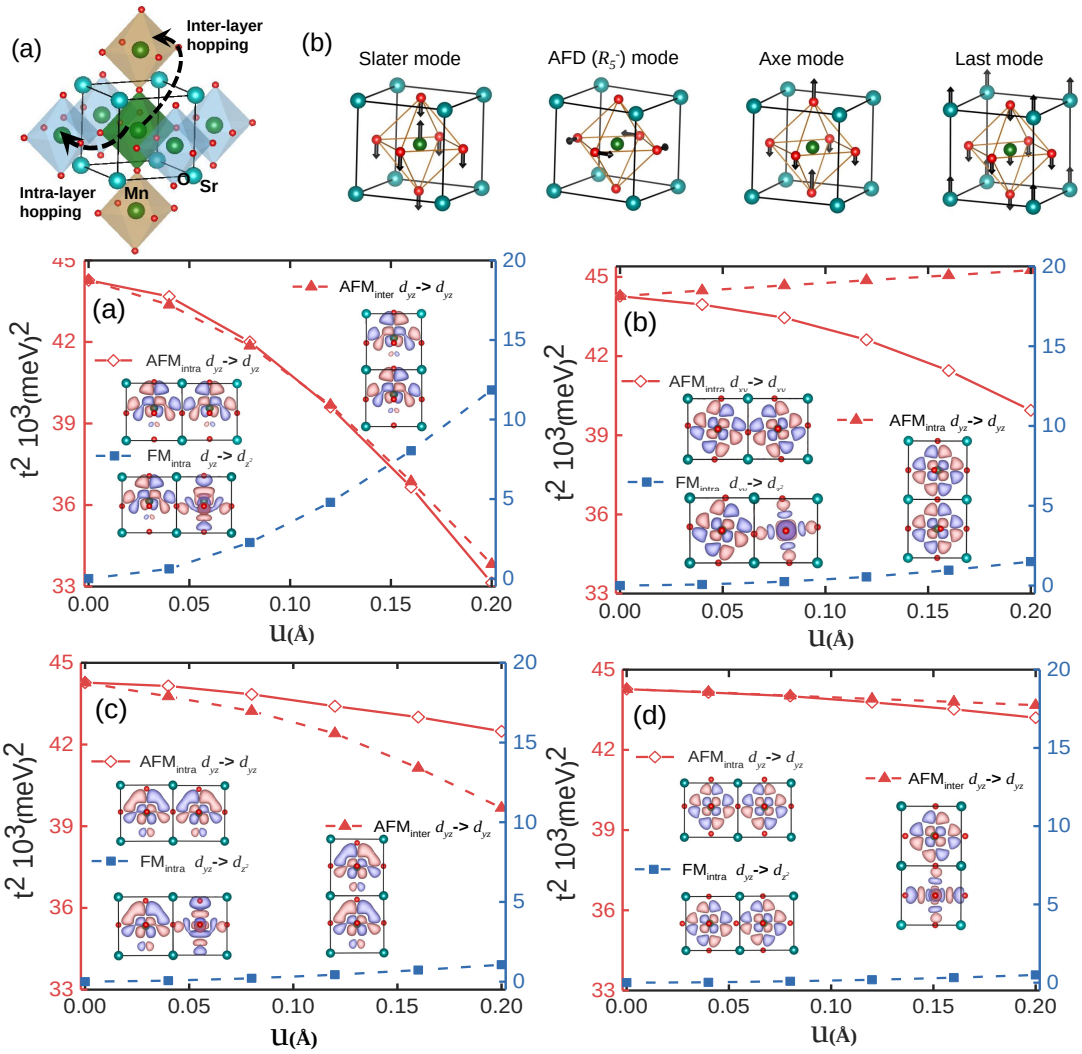

FIG. 1: (color online) (a) Schematic plots of the intra-layer and inter-layer virtual hopping processes involved in the superexchange couplings in SMO. (b) Atomic displacements of the Slater, AFD, Axe, and Last phonon modes. (c)-(f) Inter-layer and intra-layer hopping integrals involved in the AFM-type and FM-type superexchange couplings as functions of Slater, AFD, Axe, and Last phonon mode amplitudes in $SrMnO_3$ respectively. The Wannier orbitals are plotted based on the cutoff on the isosurface with charge density of 0.016 $e/bohr^3$.

ening is a general trend for all the four modes in Table I. However, the SPC strengths vary significantly with $\Delta\omega_{\rm Slater} > \Delta\omega_{\rm AFD} > \Delta\omega_{\rm Axe} > \Delta\omega_{\rm Last}$.

Let us consider the SMO with $Pm\bar{3}m$ symmetry and G-type AFM spin configuration, in which the magnetic interactions are the SE couplings between two adjacent Mn ions at site i and j. The SE interactions can be decomposed onto the contributions from intra-layer and inter-layer as schematically shown in Fig. 1(a), which denote the SE couplings through virtual hopping processes mediated by equatorial and the apical oxygen atoms on the oxygen octahedron respectively,

$$E_{\rm spin} = \sum_{i,j} \mathcal{J}^{\parallel}_{i,j} \vec{S}_i \cdot \vec{S}_j + \sum_{i,j} \mathcal{J}^{\perp}_{i,j} \vec{S}_i \cdot \vec{S}_j. \qquad (1)$$

In order to elucidate its electronic origin, we apply the recently developed extended KK model, in which the SE interactions can be expressed as[7,8]

$$\mathcal{J}_{i,j} = \sum_{\alpha,\alpha'} J^{\rm AFM}_{\alpha,\alpha'} - \sum_{\alpha,\beta} J^{\rm FM}_{\alpha,\beta} \qquad (2)$$

The first term in Eq. (2) describes the AFM-type coupling energy via a virtual hopping process between the two half-filled t_{2g} bands. The second term depicts the competing FM-type coupling energy originating from a hopping process from the half-filled t_{2g} bands to the empty e_g bands. Here, we adopt the convention to represent the AFM-type coupling and the competing FM-type coupling energies by positive and negative signs respectively. In our extended KK model, the coupling magnitude is proportional to the hopping integral t^2 and electronic screening is considered by the cRPA. Both t_{2g} and

e_g orbitals as well as their hopping integrals are constructed based on MLWFs. The details of our extended KK model can be found in Ref.[7,8].

III. RESULTS AND DISCUSSIONS

In the cubic SMO, the SE interactions are dominated by the AFM-type hopping processes from the half-filled t_{2g} orbital on one Mn atom to another t_{2g} orbital of the neighboring Mn atoms. With the t_{2g} states represented by the MLWFs, mixed oxygen $2p$ character can be identified in Fig. 1(c)-(f). This is consistent with the fact that the SE interaction is mediated by the oxygen atom. On the other hand, the FM-type hopping processes, with an opposite sign of coupling energy, are all varnishing due to the orthogonal condition in the cubic symmetry. In order to study the SPC effect, we compute the $J_{\alpha,\beta}$ as functions of various phonon modes amplitudes u that have been frozen into the cubic SMO perturbatively. As shown in Fig. 1, the quadratic dependence of the hopping integral on the phonon amplitudes enable us to use the quadratic coefficient $J^{''}_{\alpha,\beta} = \partial^2 J_{\alpha,\beta}/\partial u^2$ to measure the SPC strengths for the individual hopping process. The resulting $J^{''}_{\alpha,\beta}$ and total $J^{''}_{\rm T}$ are presented in Table I.

Consider $J^{''}_{\rm T}$ as the measure of the SPC strength, the negative values of $J^{''}_{\rm T}$ indicate that the structural distortions by all the four phonon modes suppress the AFM ordering energies, and favor the stabilization of FM spin configurations. A close inspection further reals that the magnitude of $J^{''}_{\rm T}$ thus the SPC strength decreases fast in order of Slater, AFD, Axe, and the Last mode. This feature is exactly consistent with the the first-principles results as shown in Table I. However, our method can further unveils the electronic origins that are not accessible in direct first-principles calculations as we discuss in the following.

Among all the phonon modes under investigation, the Slater mode has the largest SPC strength. Such a large SPC effect originates from the rapidly decreased SE interactions of both intra-layer coupling ($J^{''}_{\parallel}$) and inter-layer coupling ($J^{''}_{\perp}$) as shown in Table I. We first focus on the intra-layer electronic processes contributing to the SPC. Under the Slater mode, an electric dipole is generated by the relative displacements of the Mn cation and the octahedron in opposite directions along the [001] as schematically shown in Fig. 1(b). In the above, the octahedron is moving approximately rigidly together with six oxygen atoms. As a result, the intra-layer Mn-O-Mn bonds are no longer straight lines as they were in the cubic phase. Because of the above perturbed local chemical environment, the t_{2g} orbitals on two neighboring Mn atoms are distorted and tilted away from each other as shown in Fig. 1(c). Not surprisingly, the AFM-type SE coupling energies are decaying fast with the increased mode amplitude. It can be also clearly seen by the relatively large magnitudes of $J^{''}_{\parallel,(d_{xz},d_{xz})}$ and $J^{''}_{\parallel,(d_{yz},d_{yz})}$ in Table I. Since the polar distortion is along [001], the intra-layer hopping processes involving the d_{xz} and d_{yz} orbitals are thus the most effectively coupled with the Slater mode. The hopping process from $d_{xy} \rightarrow d_{xy}$ involving orbitals that spread out in the xy plane is much less affected. Therefore, it is much weakly coupled to to the Slater mode resulting in a relatively small magnitude of $J^{''}_{\parallel,(d_{xy},d_{xy})}$. Interestingly, the e_g and t_{2g} states are no longer orthogonal to each other by the broken symmetry under Slater mode. As a result, the FM-type SE coupling is now allowed and its coupling energies are increased rapidly with the mode amplitude as shown in Fig. 1(c). The above increased FM-type SE couplings, such as $J^{''}_{\parallel,(d_{xz},d_{x^2-y^2})}$, greatly contribute to the SPC effect. In the next, we discuss the inter-layer electronic processes contributing to the SPC. The only non-varnishing contributions are due to the AFM-type hoping integrals of $d_{xz} \rightarrow d_{xz}$ and $d_{yz} \rightarrow d_{yz}$ mediated by the apical oxygen atoms on the octahedron. Under the Slater mode, the Mn atom is moving closer to one of the apical oxygen atom while moving further away from the other apical oxygen atom. As a result, the hybridized oxygen $2p$ character on the d_{yz} or d_{xz} is enhanced at one end, however, significantly suppressed at the other end. Such a change in the local chemical environment reduces the effective overlap of the t_{2g} states and the SE coupling energies.

The AFD mode has the second largest SPC effect. The AFD mode is a nonpolar structural distortion describing the octahedral rotation around [001]. Under this mode, all the atomic displacements take place within the xy plane. Thus, it is expected that the SE interactions involving the t_{2g} or e_g electrons, whose main orbitals are distributed within the xy plane, will be most affected. Indeed, a close inspection in Table I reveals that the SPC effect of this mode is mainly contributed by $J^{''}_{\parallel,(d_{xy},d_{xy})}$. Under this octahedron rotation mode, the d_{xy} states on the two neighboring Mn atoms are rotated away from each other, which reduces the hopping integral and the SE coupling energy as shown in Fig. 1(d). By the same token, the FM-type hopping process between d_{xy} and the empty e_g states are no longer zero due to the symmetry breaking, which also enhance the FM-type SE couplings and contribute to the overall SPC strength.

The Axe mode has a weaker SPC effect than that of the AFD mode. As shown in Fig. 1(b), the Axe mode describe a polar distortion in which the electric dipole is generated by the relative displacements of the apical and equatorial oxygen atoms in opposite directions along [001]. In the above, the two apical oxygen atoms have a much large displacement than that of the equatorial oxygen atoms. As a result, the SE coupling via the inter-layer Mn-O-Mn hopping processes are most perturbed by the Axe mode. Indeed, the SPC effect of Axe mode are mainly contributed by the $J^{''}_{\perp,(d_{xz},d_{xz})}$ and $J^{''}_{\perp,(d_{yz},d_{yz})}$ in Table I. The above two terms describe the suppressed AFM-type SE coupling energies when the Mn atom is moving closer to one of the apical oxygen atom but leav-

TABLE I: Computed phonon frequencies ω (cm^{-1}) and their shifts $\Delta\omega(\mathrm{cm}^{-1})$ between G-AFM and FM spin orderings for Slater, AFD, Axe, and Last modes of $SrMnO_3$. For one Mn atom, $J''_{\parallel,(\alpha,\beta)}$ ($J''_{\parallel}$) and $J''_{\perp,(\alpha,\beta)}$ ($J''_{\perp}$) represent the quadratic coefficients (meV/$\mathring{A}^2$) of individual (total) intra-layer and inter-layer superexchange couplings as functions of frozen mode amplitudes for the above four modes. $J''_{\mathrm{T}} = J''_{\parallel} + J''_{\perp}$ denotes the sum of the quadratic coefficients. Values in parentheses were from Ref.[26].

	Slater Mode						AFD Mode						Axe Mode						Last Mode					
ω	G-AFM			FM		$\Delta\omega$	G-AFM			FM		$\Delta\omega$	G-AFM			FM		$\Delta\omega$	G-AFM			FM		$\Delta\omega$
	231(217)			$103i(112i)$		-334	$70i(71i)$			$112i(127i)$		-42	525(516)			518(504)		-7	172(171)			171(170)		-1
	AFM type			FM type			AFM type			FM type			AFM type			FM type			AFM type			FM type		
	d_{xy}	d_{xz}	d_{yz}	$d_{x^2-y^2}$	d_{z^2}		d_{xy}	d_{xz}	d_{yz}	$d_{x^2-y^2}$	d_{z^2}		d_{xy}	d_{xz}	d_{yz}	$d_{x^2-y^2}$	d_{z^2}		d_{xy}	d_{xz}	d_{yz}	$d_{x^2-y^2}$	d_{z^2}	
$J''_{\parallel,(\alpha,\beta)}$ d_{xy}	-8.5	0	0	0	0		-40.1	0	0	8.6	1.9		0.4	0	0	0	0		1.3	0	0	0	0	
d_{xz}	0	-39.3	0	23.2	14.7		0	-1.5	0	0	0		0	-6.1	0	0.2	1.3		0	-3.3	0	1.0	0.6	
d_{yz}	0	0	-39.3	23.2	14.7		0	0	-1.5	0	0		0	0	-6.1	0.2	1.3		0	0	-3.3	1.0	0.6	
$J''_{\perp,(\alpha,\beta)}$ d_{xy}	0	0	0	0	0		0	0	0	0	0		0	0	0	0	0		0	0	0	0	0	
d_{xz}	0	-71.6	0	0	0		0	3.1	0	0	0		0	-31.0	0	0	0		0	-4.1	0	0	0	
d_{yz}	0	0	-71.6	0	0		0	0	3.1	0	0		0	0	-31.0	0	0		0	0	-4.1	0	0	
$J''_{\parallel}$	-326.1						-107.1						-29.9						-16.6					
$J''_{\perp}$	-143.2						6.1						-62.0						-4.9					
J''_{T}	-469.3						-101.0						-91.9						-21.4					

ing away from the other one.

Finally, we discuss the SPC effect by Last mode, which is the weakest among all. This is due to the nature of the Last mode, in which an electric dipole is generated by the displacements of the A-site atom moving in [001] direction and the octahedron with all six oxygen atoms and the Mn atom together moving in $[00\bar{1}]$ direction as schematically shown in Fig. 1(b). Such a structural distortion barely modifies the local Mn-O bonding environment, which is crucial for the SE coupling energy. As a result, both the t_{2g} and the e_g orbitals are nearly intact due to the rigid displacement of the entire octahedron shown in Fig. 1(f). Not surprisingly, the SE coupling are not changed resulting in a rather weak SPC effect.

TABLE II: The quadratic coefficients (meV/$\mathring{A}^2$) of individual(total) $J''_{\parallel,(\alpha,\beta)}$ ($J''_{\parallel}$) intra-layer and $J''_{\perp,(\alpha,\beta)}$ ($J''_{\perp}$) inter-layer superexchange couplings as functions of frozen mode amplitudes for the Slater mode in $BiFeO_3$.

AFM type		d_{xy}	d_{yz}	d_{zx}	$d_{x^2-y^2}$	d_{z^2}	
$J''_{\parallel,(\alpha,\beta)}$	d_{xy}	-4.0	$\sim$0	0	0	0	$J''_{\parallel}$ = -5.7
	d_{yz}	$\sim$0	-18.2	0	17.6	9.2	
	d_{zx}	0	0	-18.2	17.6	9.2	
	$d_{x^2-y^2}$	0	30.4	30.4	-46.6	-26.0	
	d_{z^2}	0	15.9	15.9	-26.0	-12.9	
$J''_{\perp,(\alpha,\beta)}$	d_{xy}	$\sim$0	0	0	0	0	$J''_{\perp}$ = -64.3
	d_{yz}	0	-20.1	0	0	0	
	d_{zx}	0	0	-20.1	0	0	
	$d_{x^2-y^2}$	0	0	0	$\sim$0	0	
	d_{z^2}	0	0	0	0	-24.1	

Based on the GKA theory, the metal-oxygen-metal angle has often been applied as a thumb of rule to explain the SPC effect. Indeed, part of our analysis in the Slater mode and AFD modes is consistent with the expectation from this rule. In fact, Slater mode and AFD mode are the two phonon modes that directly change the Mn-O-Mn angles and they are also identified to have the strongest SPC effect. Yet, the fact that slater mode has a much larger SPC effect than that of AFD mode can not be satisfactorily explained by this phenomenological rule only, since they adjust the Mn-O-Mn angle by a similar magnitude[8]. Our current analysis provides a clearer electronic insight into the above discrepancy. It shows that the Slater mode has a greater number of effectively coupled hopping processes than AFD mode, which are crucially dependent on the symmetry of crystal field splitting. In addition, the SPC in Slater mode benefits further from the inter-layer coupling. In the above, the Mn-O-Mn remains a straight line, but the oxygen atom displaces from the unperturbed symmetric position. This effect is not captured by the Mn-O-Mn angle.

The SPC effect in perovskite BFO appears even more elusive to the phenomenological rule based on Fe-O-Fe angles. One would expect that the SPC of Slater mode should be comparable to that in SMO, since the characteristic of the mode is similar to that in SMO. On the contrary, first-principles calculations show a very weak SPC effect, in which the frequency shift between AFM and FM spin configurations is only $\Delta\omega = 3\ \mathrm{cm}^{-1}$. This seemingly discrepancy can be easily explained by the analysis developed in this work. In Table II, we present the similar quantities of J'' as a measure of the SPC strengths from various electronic hopping processes in BFO. As we have discussed earlier, the large SPC effect of Slater mode in SMO benefits from both the rapidly suppressed AFM-type SE interaction between two half-filled d states and the same rapid increased FM-type SE interaction between one half-filled d state to the empty d state. In

sharp contrast to the electronic configuration of Mn^{3+} in SMO with half-filled t_{2g} and empty e_{2g} states, the Fe^{3+} in BFO has both t_{2g} and e_{2g} states being half-filled. As a result, only AFM-type SE couplings in Eq. 2 are allowed in BFO. The FM-type hopping processes from t_{2g} to e_{2g} which contribute significantly to the SPC effect of Slater mode in SMO now change their signs of energy as shown in Eq. 2 and become AFM-type. Instead of promoting SPC effect in SMO, those SE coupling channels now largely suppress the SPC in BFO as shown by the negative values of $J''_{\alpha,\beta}$ from t_{2g} to e_{2g} hopping processes in Table II. Therefore, the intra-layer coupling $J''_{\parallel}$ is much smaller for Slater mode in BFO than in SMO.

IV. CONCLUSION

In conclusion, we have studied the electronic origins of the SPC effect in transition metal perovskite by using the Wannier-based extended Kugel-Khomskii model. It shows that the number of effectively coupled electronic hopping processes is the key in the SPC strength. Those effectively coupled magnetic interactions are crucially dependent on both the characteristic of the phonon mode and the d orbitals in the crystal splitting field. The phonon mode such as the Slater mode which affects almost every metal-oxygen hybridization environment will maximize the SPC effect. Following the same picture, it will not be difficult to understand that the "Slater-like" mode (Γ_1^-) is found to have strong SPC in double perovskite La_2NiMnO_6[8]. The electronic configurations are important as well, which are at variance in perovskite materials with different B-site cations. The empty d states of Mn atom in SMO play the decisive role in the fact that its SPC effect is much stronger than that in BFO with all half-filled d states. Following the above argument, the much larger SPC effect in $LaCrO_3$ than that in $LaFeO_3$[8,26] reported in literature is not surprising. In addition, a recent experiment in Bi_2FeCrO_6[41] suggested a spin-phonon coupling could be induced when the empty d states are introduced by Cr to replace Fe, which is also consistent with our conclusion.

V. ACKNOWLEDGMENTS

This work was supported as part of the Center for the Computational Design of Functional Layered Materials, an Energy Frontier Research Center funded by the U.S. Department of Energy, Office of Science, Basic Energy Sciences under Award no. DE-SC0012575 (Both X. W. and L. H. designed the project). L.H. was supported by the Chinese National Science Foundation Grant number 11374275, and the National Key Research and Development Program of China under Grants No. 2016YFB0201200 (H.W. , X.W.and L.H. constructed the extended Kugel-Khomskii model). H. J. was supported by the National Natural Science Foundation (Project Nos. 21373017, 21321001) and Ministry of Science and Technology (2013CB933400) of China (H. W. and H. J. carried out the calculations within constrained random phase approximation). XW is partially supported by the National Science Foundation (NSF), DMR under Award No. DMR-1552287 (supervision of undergraduate research performed by C. S.). This research used resources of the National Energy Research Scientific Computing Center (NERSC), a DOE Office of Science User Facility supported by the Office of Science of the U.S. Department of Energy under Contract No. DE-AC02-05CH11231.

* To whom correspondence should be addressed: xifanwu@temple.edu, and helx@ustc.edu.cn.

[1] N. A. Spaldin, S. W. Cheong, and R. Ramesh, Phys. Today **63**, No. 10, 38 (2010).
[2] C. J. Fennie and K. M. Rabe, Phys. Rev. Lett. **96**, 205505 (2006).
[3] C. J. Fennie and K. M. Rabe, Phys. Rev. Lett. **97**, 267602 (2006).
[4] T. Birol and C. J. Fennie, Phys. Rev. B **88**, 094103 (2013).
[5] J. H. Lee et al., Nature **466**, 954-958 (2010).
[6] Y. Tokura, S. Seki, and N. Nagaosa, Rep. Prog. Phys. **77**, 076501 (2014).
[7] H. Wang, I. V. Solovyev, W. Wang, X. Wang, P. J. Ryan, D. J. Keavney, J.-W. Kim, T. Z. Ward, L. Zhu, J. Shen, X. M. Cheng, L. He, X. Xu, and X. Wu, Phys. Rev. B **90**, 014436 (2014).
[8] See Supplemental Material [url] for on the computational details, theoretical model and calculation, which includes Ref.[9–14]
[9] G. Kresse and J. Furthmüller, Phys. Rev. B **54**, 11169 (1996).
[10] J. P. Perdew, A. Ruzsinszky, G. I. Csonka, O. A. Vydrov, G. E. Scuseria, L. A. Constantin, X. Zhou, and K. Burke, Phys. Rev. Lett. **100**, 136406 (2008).
[11] C. Loschen, J. Carrasco, K. M. Neyman, and F. Illas, Phys. Rev. B **75**, 035115 (2007).
[12] A. Togo and I. Tanaka, Scripta Materialia **108**, 1–5 (2015).
[13] K. Schwarz, P. Blaha, and G.K.H. Madsen, Comput. Phys. Comm. **147**, 1–2 (2002).
[14] J. Kuneš, R. Arita, P. Wissgott, A. Toschi, H. Ikeda, and K. Held, Comput. Phys. Comm. **181**, 11 (2010).
[15] H. Das, A. L. Wysocki, Y. Geng, W. Wu, and C. J. Fennie, Nat. Commun. **5**, 2998 (2014).
[16] C. J. Fennie and K. M. Rabe, Phys. Rev. B **72**, 100103 R (2005).
[17] S. Bhattacharjee, E. Bousquet, and P. Ghosez, Phys. Rev. Lett. **102**, 117602 (2009)
[18] J. H. Lee and K. M. Rabe, Phys. Rev. Lett. **104**, 207204 (2010).
[19] J. H. Lee and K. M. Rabe, Phys. Rev. Lett. **107**, 067601 (2011).
[20] S. Kamba, V. Goian, V. Skoromets, J. Hejtmánek, V. Bov-

tun, M. Kempa, F. Borodavka, P. Vaněk, A. A. Belik, J. H. Lee, O. Pacherová, and K. M. Rabe, Phys. Rev. B **89**, 064308 (2014).
[21] V. Goian, S. Kamba, F. Borodavka, D. Nuzhnyy, M. Savinov, and A. A. Belik, J. Appl. Phys. **117**, 164103 (2015).
[22] H. Wang, L. He, and X. Wu, EuroPhys. Lett. **100**, 17005 (2012).
[23] H. Das, U. V. Waghmare, T. Saha-Dasgupta, and D. D. Sarma, Phys. Rev. Lett. **100**, 186402 (2008).
[24] T. Birol, N. A. Benedek, H. Das, A. L. Wysocki, A. T. Mulder, B. M. Abbett, E. H. Smith, S. Ghosh, and C. J. Fennie, Curr. Opin. Solid State Mater. Sci. **16**, 5 (2012).
[25] J. H. Lee and K. M. Rabe, Phys. Rev. B **84**, 104440 (2011).
[26] J. Hong, A. Stroppa, J. Íñiguez, S. Picozzi, and D. Vanderbilt, Phys. Rev. B **85**, 054417 (2012).
[27] P. Garcia-Fernandez, J. A. Aramburu, and M. Moreno, Phys. Rev. B **83**, 174406 (2011).
[28] S. Cheong and M. Mostovoy, Nature Materials **6**, 13-20 (2007).
[29] S. Kamba, D. Nuzhnyy, M. Savinov, J. Šebek, J. Petzelt, J. Prokleška, R. Haumont, and J. Kreisel, Phys. Rev. B **75**, 024403 (2007).
[30] J. B. Goodenough, Phys. Rev. **100**, 564 (1955).
[31] J. Kanamori, J. Phys. Chem. Solids **10**, 87-98 (1959).
[32] K. I. Kugel and D. I. Khomskii, Sov. Phys. Usp. **25**, 231 (1982).
[33] I. Souza, N. Marzari, and D. Vanderbilt, Phys. Rev. B **65**, 035109 (2001).
[34] N. Marzari, A. A. Mostofi, J. R. Yates, I. Souza, and David Vanderbilt, Rev. Mod. Phys. **84**, 1419 (2012).
[35] L. Vaugier, H. Jiang, and S. Biermann, Phys. Rev. B **86**, 165105 (2012).
[36] J. C. Slater, Phys. Rev. **78**, 748 (1950).
[37] J. T. Last, Phys. Rev. **105**, 1740 (1957).
[38] J. D. Axe, Phys. Rev. **157**, 429 (1967).
[39] P. M. Woodward, Acta Cryst. B**53**, 32-43 (1997).
[40] H. Wang, J. Wen, D. J. Miller, Q. Zhou, M. Chen, H. N. Lee, K. M. Rabe, and X. Wu, Phys. Rev. X **6**, 011027 (2016).
[41] S. Kamba, D. Nuzhnyy, R. Nechache, K. Závěta, D. Nižňanský, E. Šantavá, C. Harnagea, and A. Pignolet, Phys. Rev. B **77**, 104111 (2008).